



## 4-Oxoquinolines and monoamine oxidase: When tautomerism matters



Francesco Mesiti <sup>a, b, c</sup>, Annalisa Maruca <sup>a, b</sup>, Vera Silva <sup>c, d</sup>, Roberta Rocca <sup>b, e</sup>,  
 Carlos Fernandes <sup>c</sup>, Fernando Remião <sup>d</sup>, Eugenio Uriarte <sup>f, g</sup>, Stefano Alcaro <sup>a, b, \*\*\*</sup>,  
 Alexandra Gaspar <sup>c, \*\*</sup>, Fernanda Borges <sup>c, \*</sup>

<sup>a</sup> Dipartimento di Scienze Della Salute, Università "Magna Græcia" di Catanzaro, Campus Universitario "S. Venuta", Viale Europa, Loc. Germaneto, 88100, Catanzaro, Italy

<sup>b</sup> Net4Science Srl, Spin-off Accademico, Viale Europa, Loc. Germaneto, 88100, Catanzaro, Italy

<sup>c</sup> CIQUP, Departamento de Química e Bioquímica, Faculdade de Ciências, Universidade Do Porto, Porto, 4169-007, Portugal

<sup>d</sup> UCIBIO-REQUIMTE, Laboratório de Toxicologia, Departamento de Ciências Biológicas, Faculdade de Farmácia, Universidade Do Porto, 4050-313, Porto, Portugal

<sup>e</sup> Dipartimento di Medicina Clinica e Sperimentale, Università "Magna Græcia" di Catanzaro, Campus Universitario "S. Venuta", Viale Europa, Loc. Germaneto, 88100, Catanzaro, Italy

<sup>f</sup> Departamento Química Orgánica, Facultad de Farmacia, Universidad de Santiago de Compostela, Campus Vida, 15782, Santiago de Compostela, España, Spain

<sup>g</sup> Instituto de Ciencias Químicas Aplicadas, Universidad Autonoma de Chile, Av. Libertador Bernardo O'Higgins, 7500912, Santiago de Chile, Chile

### ARTICLE INFO

#### Article history:

Received 15 November 2020

Received in revised form

29 December 2020

Accepted 8 January 2021

Available online 13 January 2021

#### Keywords:

Quinolone

Tautomerism

2D-Heteronuclear NMR

Human monoamine oxidases

Enzyme-ligand complexes

### ABSTRACT

4-Oxoquinoline derivatives have been often used in drug discovery programs due to their pharmacological properties. Inspired on chromone and 4-oxoquinoline chemical structure similarity, a small series of quinoline-based compounds was obtained and screened, for the first time, toward human monoamine oxidases isoforms. The data showed the *N*-(3,4-dichlorophenyl)-1-methyl-4-oxo-1,4-dihydroquinoline-3-carboxamide **10** was the most potent and selective MAO-B inhibitor ( $IC_{50} = 5.30 \pm 0.74$  nM and  $SI \geq 1887$ ). The data analysis showed that prototropic tautomerism markedly influences the biological activity. The unequivocal characterisation of the quinoline tautomers was performed to understand the attained data. To our knowledge, there have been no prior reports on the characterisation of quinolone tautomers by 2D NMR techniques, namely by  $^1H-^{15}N$  HSQC and  $^1H-^{15}N$  HMBC, which are proposed as expedite tools for medicinal chemistry campaigns. Computational studies on enzyme-ligand complexes, obtained after MM-GBSA calculations and molecular dynamics simulations, supported the experimental data.

© 2021 Elsevier Masson SAS. All rights reserved.

### 1. Introduction

4-Oxoquinolines or simply 4-quinolones are a class of natural and synthetic heterocycles that present an extensive array of pharmacological activities associated with infection, pain, ischemia, immunomodulation, inflammation, and cancer events

\* Corresponding author. CIQUP/Department of Chemistry and Biochemistry, Faculty of Sciences, University of Porto, 4169-007, Porto, Portugal.

\*\* Corresponding author. CIQUP/Department of Chemistry and Biochemistry, Faculty of Sciences, University of Porto, 4169-007, Porto, Portugal.

\*\*\* Corresponding author. Department of Health Sciences, University "Magna Græcia" of Catanzaro, 88100, Catanzaro, Italy.

E-mail addresses: [alcaro@unizc.it](mailto:alcaro@unizc.it) (S. Alcaro), [alexandra.gaspar@fc.up.pt](mailto:alexandra.gaspar@fc.up.pt) (A. Gaspar), [fborges@fc.up.pt](mailto:fborges@fc.up.pt) (F. Borges).

[1,2].

From the drug discovery programs based on 4-oxoquinoline core, several drugs were approved by Food and Drug Administration (FDA), for instance, the antimicrobials Ciprofloxacin and Elvitegravir and more recently Ivacaftor for the treatment of cystic fibrosis (Fig. 1) [3]. However, few works described their potential for neurodegenerative disorders [4–7].

Monoamine oxidases (MAOs) are FAD-dependent enzymes that exist in mammals in two isoforms, MAO-A and MAO-B. They have a key role in the regulation of monoamine neurotransmitters in the central nervous system (CNS) [8]. The MAO-B expression and activity enhance during the ageing process and represents a valid target for the therapy of neurodegenerative diseases, such as Parkinson and Alzheimer [9,10]. Irreversible MAO-B inhibitors (IMAO-

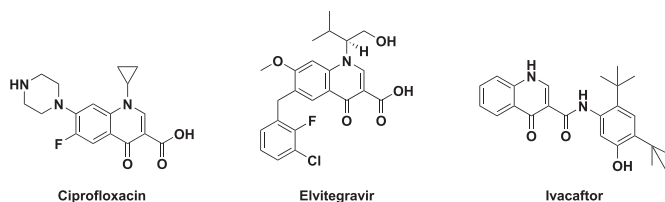


Fig. 1. 4-Oxoquinoline-based drugs.

B) were, until FDA approval of safinamide in 2017, the first-line drugs used in the adjunctive treatment of Parkinson's disease (PD). However, due to reported drugs side-effects, the discovery of reversible and selective IMAO-B is still a relevant issue.

In recent years, our research has been focused on chromone (1,4-benzopyrone) as a privileged scaffold for the development of monoamine oxidase inhibitors. Our structure-activity relationship (SAR) studies on this type of molecules allow lead optimisation through a selection of chemical modifications aimed to improve affinity and/or selectivity [11–13]. The second stage of the project was to map pharmacophore features of the most potent, selective, and reversible MAO-B inhibitor by bioisosteric and scaffold hopping approaches. These methods are often used in medicinal chemistry to change structural fragments with other chemical features or to diversify the scaffold space to improve activity, reduce toxicity, change pharmacokinetic properties without a significant perturbation in the activity profile [14].

Inspired by chromone and 4-oxoquinoline chemical structure similarity, in this work we report the design and synthesis of a small set of 4-oxoquinoline-based compounds based on the most potent and selective chromone-based IMAO-B described by Reis et al. (Fig. 2) [12] As far as we know, only a few 4-oxoquinoline derivatives were screened towards MAOs [15,16].

After synthesis, the compounds were screened toward human MAOs isoforms (*h*MAO-A and *h*MAO-B) and the cytotoxic outline of the best compounds was evaluated in differentiated human neuroblastoma (SH-SY5Y) cell lines. Molecular docking studies were also performed to provide insights on ligand-enzyme interactions at a molecular level.

## 2. Results and discussion

### 2.1. Chemistry

The *N*-phenyl-4-oxoquinoline-3-carboxamide derivatives 2–4 were synthesised in satisfactory yields (35–80%) by a one-pot condensation reaction that occurred between 4-oxoquinoline-3-carboxylic acid (compound 1, Scheme 1) and 3,4-dimethylaniline, 3-chloroaniline, or 3,4-dichloroaniline in alkaline conditions (DIPEA) (Scheme 1). The coupling reagent selected for the carboxylic acid activation was 2-(1H-benzotriazole-1-yl)-1,1,3,3-tetramethylammonium tetrafluoroborate (TBTU) [17]. Phosphoryl chloride (POCl<sub>3</sub>), often used in the synthesis of chromone-derivatives [12], was found not suitable for the synthesis of these type of amides due to the formation of numerous side products [18].

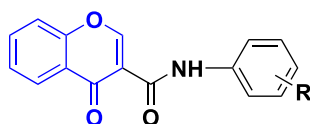
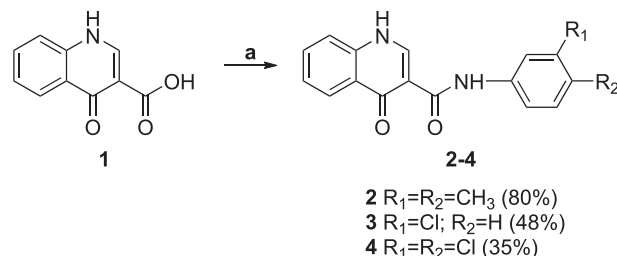


Fig. 2. General structure of chromone-based IMAO-B studied by Reis et al. [12].



Scheme 1. Synthesis of *N*-phenyl-4-oxoquinoline-3-carboxamide derivatives 2–4. Reagents and conditions: (a) TBTU, DIPEA, DMF, appropriate amine, rt, overnight.

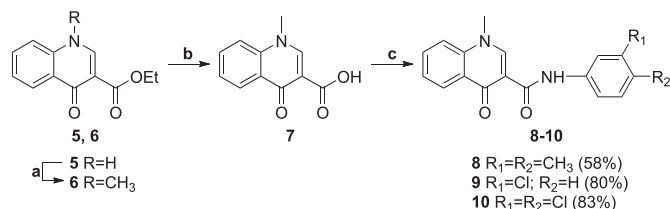
The *N*-methyl-4-oxoquinoline derivatives 8–10 were synthesised by a two-step synthetic route, as the starting carboxylic acid was not commercially available (Scheme 2). Firstly, the ethyl-4-oxoquinoline-3-carboxylate 5 was obtained from aniline and diethyl ethoxymethylenemalonate (DEEMM) by a Gould-Jacobs reaction. Then, the enaminoester intermediate was subjected to a thermal driven intramolecular cyclisation in diphenyl ether [19]. The ester derivative 5 was alkylated with methyl iodide to provide the *N*-methyl derivative 6 (Scheme 2, step a). After alkaline hydrolysis (NaOH) the corresponding carboxylic acid 7 was obtained (Scheme 2, step b) [17,20]. The *N*-methyl-4-oxoquinoline derivatives 8–10 were obtained in good yields by amidation of compound 7 with the appropriate aniline (3,4-dimethylaniline, 3-chloroaniline, and 3,4-dichloroaniline) using TBTU as coupling agent (Scheme 2, step c) [3].

The structural elucidation of all compounds was performed by NMR spectroscopy (<sup>1</sup>H, <sup>13</sup>C and DEPT-135) and electronic impact mass spectrometry (EI-MS). Similar data (primarily based on H-2, NH, and C-4 chemical shifts) was described for other *N*-phenyl-4-oxoquinoline-3-carboxamides, namely ivacaftor [3].

### 2.2. Monoamine oxidase inhibition studies

The MAOs inhibition profile of the *N*-phenyl-4-oxoquinoline-3-carboxamide (2–4) and *N*-phenyl-1-methyl-4-oxoquinoline-3-carboxamide (8–10) derivatives was evaluated by a spectrophotometric assay using kynuramine as substrate and recombinant *h*MAO-A and *h*MAO-B isoforms [21]. The results of the *h*MAOs inhibition activity (IC<sub>50</sub> values) and selectivity (SI) of compounds 2–4, compounds 8–10 and reference drug inhibitors (rasagiline and safinamide for *h*MAO-B, clorgyline for *h*MAO-A) are depicted in Table 1.

The biological results showed that derivatives 2–3 were not active at the highest concentration tested (10 μM) and that the derivative 4 displayed a *h*MAO-B IC<sub>50</sub> value (IC<sub>50</sub> = 11.1 ± 0.9 nM) approximately two-fold lower than safinamide. Furthermore, compound 4 showed a weak inhibitory activity towards *h*MAO-A (IC<sub>50</sub> = 1743 ± 146 nM) with a selectivity index (SI) of 157. On the other hand, the *N*-methyl derivatives 8 and 9 exhibited inhibitory



Scheme 2. Synthesis of *N*-phenyl-1-methyl-4-oxoquinoline-3-carboxamide derivatives 8–10. Reagents and conditions: (a) CH<sub>3</sub>I, K<sub>2</sub>CO<sub>3</sub>, DMF, 60 °C, 1 h, argon; (b) NaOH (aq), reflux, 4 h; (c) TBTU, DIPEA, DMF, appropriate amine, rt, overnight.

**Table 1**

hMAOs inhibitory activities of *N*-phenyl-4-oxoquinoline-3-carboxamide (2–4) and *N*-phenyl-1-methyl-4-oxoquinoline-3-carboxamide (8–10) derivatives and reference inhibitors (Rasagiline, Safinamide, and Clorgyline).

Compound	IC <sub>50</sub> (nM)		SI <sup>a</sup>
	hMAO-B	hMAO-A	
2	35% <sup>b</sup>	15% <sup>b</sup>	–
3	40% <sup>b</sup>	8% <sup>b</sup>	–
4	11.1 ± 0.9	1743 ± 146	157.0
8	82.3 ± 9.1	1611 ± 65	19.6
9	29.0 ± 1.5	7482 ± 1506	258.0
10	5.3 ± 0.7	38% <sup>b</sup>	≥1887 <sup>c</sup>
Rasagiline	45.7 ± 3.0	2340 ± 125	51.2
Safinamide	25.3 ± 1.8	13% <sup>b</sup>	≥395.1 <sup>c</sup>
Clorgyline	2212 ± 264	3.2 ± 0.2	0.001

<sup>a</sup> Selectivity Index (SI = IC<sub>50</sub>(hMAO-A)/IC<sub>50</sub>(hMAO-B)).

<sup>b</sup> Percentage of inhibition at 10 μM (highest concentration tested).

<sup>c</sup> Values obtained under the assumption that the corresponding IC<sub>50</sub> against hMAO-A is the highest concentration tested (10 μM). Results are represented as mean ± SD from at least three independent experiments, performed in triplicate.

activity towards both hMAOs (compound 8 hMAO-B IC<sub>50</sub> = 82.3 ± 9.1 nM and hMAO-A IC<sub>50</sub> = 1611 ± 65 nM; compound 9 hMAO-B IC<sub>50</sub> = 29.0 ± 1.5 nM and hMAO-A IC<sub>50</sub> = 7482 ± 1506 nM) and a SI of 19.6 and 258, respectively. Noteworthy, compound 10 was the most potent and selective IMAO-B (IC<sub>50</sub> = 5.3 ± 0.7 nM and SI: ≥1887).

Taken into account the previous data of our group on chromone-3-carboxamides [12,13], the results obtained were quite intriguing. In fact, we expected that, due to structural analogy, *N*-phenyl-4-oxoquinoline-3-carboxamides 2–4 followed the same trend as the equivalent chromone-based IMAO-B. Moreover, it was predictable that the activity of derivatives 8–10 was compromised by the presence of the *N*-methyl moiety considering the shape of the active pocket of MAO-B [22]. The unexpected biological data drive us to an in-depth structural study on 4-oxoquinoline system. Thus, we postulated that tautomerism of 4-oxoquinolines can somehow influences the MAOs inhibition profile of the ligands. Therefore, additional studies were carried out to rationalise the data obtained.

### 3. 4-Oxoquinoline tautomerism

The structural elucidation of 4-oxoquinoline derivatives has been carried out by several analytical methodologies, mainly UV, IR, X-ray crystallography, and NMR [23–26]. However, despite the large data set, the structural characterisation of 4-oxoquinoline tautomers (Fig. 3A) is somewhat ambiguous. Almost all reported NMR data were recorded in DMSO-*d*<sub>6</sub>, possibly due to solubility constraints of the bicyclic structures, and the prevalence of the 4-oxo tautomer is proposed [3,26,27]. However, Wentrup and co-workers [28] showed by NMR that for 2-substituted-4-oxoquinolines, the presence of 4-hydroxy tautomer is favoured in DMSO-*d*<sub>6</sub> while the 4-oxo tautomer is observed in CDCl<sub>3</sub>.

Nevertheless, besides the influence of the polarity and hydrogen binding ability of the solvents used in NMR [26,29,30] other factors

can disturb the tautomeric equilibrium, namely the type of substituents located in the 4-oxoquinoline scaffold [27,29,31]. It has been described that the 4-hydroxy tautomer is favoured in systems bearing hydrogen bond acceptors at position C-3, such as a carboxyl group, as observed for the 4-hydroxyquinoline-3-carboxylic acid and its derivatives [26,27,31]. On the contrary, the 4-oxo tautomer was described as prevalent in quinolone systems enclosing electron-withdrawing groups at position C-2 [26,29]. This type of tautomerism was also described for 4-pyridones and 4-hydroxypyridines [30,32].

Generally, the NMR assignments of the 4-oxo or 4-hydroxyquinoline tautomers are largely based on the chemical shifts of H-2 or H-3, NH and C-4 atoms [27,31,33–36]. Based on the NMR data, several groups claim that the occurrence of 4-oxo or 4-hydroxy tautomers can be unquestionably ascribed to the chemical shift of C-4, being the signals at δ<sub>C</sub> ≥ 170 ppm attributed, in general, to the C-4 bearing a carbonyl group [27,31,35,36].

Taken in mind the data attained in our enzymatic assays and the possibility of the existence of 4-oxo and 4-hydroxy tautomers in the compounds 2–4, which is blocked in the case of their *N*-methyl counterparts 8–10, a systematic NMR study was carried out. To note that all the efforts to obtain suitable crystals for X-ray analysis have failed.

#### 3.1. NMR analysis of 4-oxoquinoline-3-carboxylic acid (compound 1)

The first step of our studies was focused on the NMR characterisation of the starting material 4-oxoquinoline-3-carboxylic acid (compound 1, Fig. 3B). The study was performed with the 4-oxoquinoline-3-carboxylic acid purchased from Fluorochem (CAS number: 13721-01-2), and the 4-hydroxy tautomer (4-hydroxyquinoline-3-carboxylic acid, CAS Number: 34785-11-0) acquired to Sigma-Aldrich (Fig. 3B). The <sup>1</sup>H and <sup>13</sup>C NMR (DMSO-*d*<sub>6</sub>) spectra of both compounds were recorded in the same experimental conditions and at the same concentration (10 mg/700 μL). When compared a perfect spectral correspondence was obtained, which indicates the presence of the same type of tautomer in solution (Table 2). Spectral matching was also observable by FT-IR, reinforcing the statement that both compounds are in the same tautomeric form (Figure S1, supporting information).

In the <sup>1</sup>H NMR it was observed the presence of a high downfield broad signal (1H; δ = 15.38 ppm) suggesting that an intramolecular hydrogen bond, is present although we cannot distinguish if it is a OH...N or an O...NH bond. From the <sup>13</sup>C NMR data, two downfield signals at δ = 178.2 and 166.3 ppm were observed that can be assigned to the function located at position 4 (carbonyl or hydroxyl). The spectra showed the presence of ten carbons, which indicate the presence of only one tautomer in solution. Then, 1D (DEPT) and 2D (COSY, HSQC and HMBC) NMR experiments were accomplished, and some signals were unequivocally assigned (Table 2). However, after the spectra analysis, the doubts related to the type of tautomer present in solution remained.

Therefore, 2D-NMR experiments using <sup>15</sup>N heteronuclear correlations were performed as they can figure out the existence of N–H interactions. As no correlation was noticed in the <sup>1</sup>H–<sup>15</sup>N HSQC we conclude that the 4-hydroxy tautomer is the only species present in solution. The data was corroborated by <sup>1</sup>H–<sup>15</sup>N HMBC (Fig. 4), which revealed the presence of long-range interactions between the nitrogen at δ = 150.6 ppm, and the hydrogen signals at δ = 8.90 ppm (s), and δ = 7.83 ppm (dd, *J* = 8.3, 1.3 Hz), which were assigned as H-2 and H-8, respectively (Table 2). The nitrogen signal at δ = 150.6 ppm, when compared with the values obtained for similar systems [22] is upfield due to the presence of an intramolecular hydrogen bond (Fig. 3B). No traces of 4-oxoquinoline

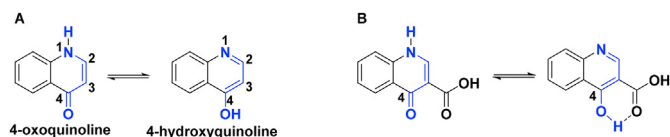


**Fig. 3.** (A) Structure, numbering, and tautomeric equilibrium of 4-oxoquinoline and (B) 4-oxoquinoline-3-carboxylic acid.

**Table 2**  
<sup>1</sup>H, <sup>13</sup>C, and <sup>13</sup>C-<sup>1</sup>H HMBC spectroscopic data of compound 1.

Atom number	Chemical shifts (ppm, DMSO- <i>d</i> <sub>6</sub> )		HMBC correlations
	$\delta^1\text{H}$ (mult, <i>J</i> , Hz)	$\delta^{13}\text{C}$	
2	8.90 (s)	<u>145.2</u> <sup>a</sup>	107.5 (C-3); 166.3 (COOH); 178.2 (C-4)
3	—	107.5 <sup>b</sup>	
4	—	178.2 <sup>b,c</sup>	
4a	—	139.5 <sup>b</sup>	
5	8.31 (dd, <i>J</i> = 8.1, 1.1)	<u>124.9</u> <sup>a</sup>	139.5 (C-4a); 178.2 (C-4)
6	7.90 (ddd, <i>J</i> = 8.1, 6.9, 1.4)	<u>133.8</u> <sup>a</sup>	139.5 (C-4a);
7	7.61 (ddd, <i>J</i> = 8.3, 6.9, 1.1)	<u>133.8</u> <sup>a</sup>	124.3 (C-8a)
8	7.83 (d, <i>J</i> = 8.3)	<u>119.7</u> <sup>a</sup>	124.3 (C-8a); 178.2 (C-4)
8a	—	124.3 <sup>b</sup>	
COOH	15.38 (s)	<u>166.3</u> <sup>b,c</sup>	

Distortionless enhancement by polarization transfer (DEPT) signals are reported as underlined values.

<sup>a</sup> Assignment based on the <sup>1</sup>H-<sup>13</sup>C-HSQC data.

<sup>b</sup> Assignment based on the <sup>1</sup>H-<sup>13</sup>C-HMBC data.

<sup>c</sup> Assignment based on the <sup>1</sup>H-<sup>15</sup>N HMBC data.

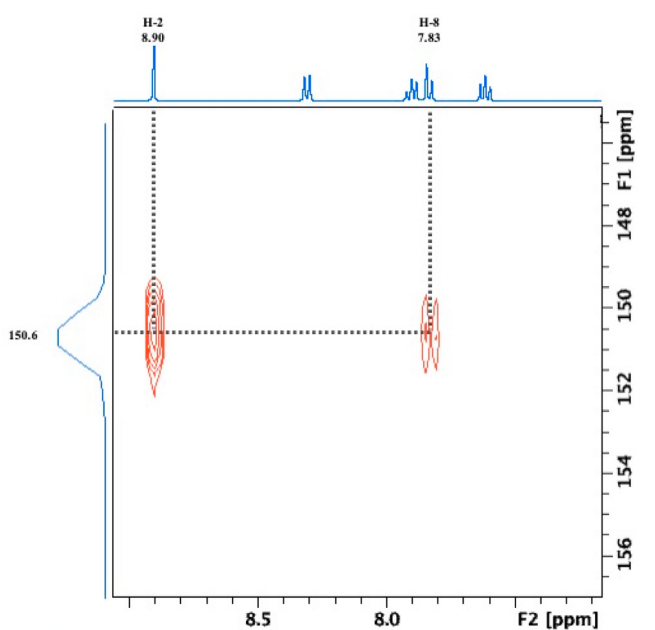
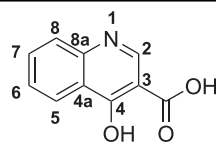


**Fig. 4.** Expansion of the <sup>1</sup>H-<sup>15</sup>N HMBC spectrum of compound 1.

tautomer were found in the spectral analysis.

### 3.2. NMR analysis of *N*-phenyl-4-oxoquinoline-3-carboxamides (2–4)

The same workflow described previously for the NMR analysis of 4-oxoquinoline-3-carboxylic acid was followed for the complete structural elucidation of compounds 2–4. In particular, the data obtained from 1D NMR analysis for the principal diagnostic/informative peaks (<sup>1</sup>H and <sup>13</sup>C) are reported in Table 3. Furthermore, the complete data obtained from 1D (DEPT) and 2D NMR (COSY, HSQC, and HMBC), analysis is presented in Table S1 supporting information.

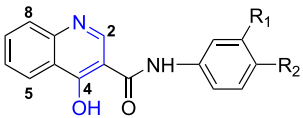
The <sup>1</sup>H-<sup>15</sup>N HSQC experiments showed the presence of only one

*N*-H direct correlation signal. In compound 2, for example, it occurred between the nitrogen signal at  $\delta = 131.8$  ppm and the hydrogen at  $\delta = 12.35$  ppm (Fig. 5A, Table 4). In the <sup>1</sup>H-<sup>15</sup>N HMBC spectrum, a long-range interaction between the nitrogen at  $\delta = 143.6$  ppm and the hydrogens at  $\delta = 8.85$  ppm (H-2, s) and at  $\delta = 7.75$  ppm (H-8, dd, *J* = 8.4, 1.2 Hz) was detected (Fig. 5B, Table 4). Accordingly, the signal at  $\delta = 143.6$  ppm was assigned as the nitrogen of the 4-hydroxyquinoline moiety and the signals at  $\delta = 12.35$  ppm and at  $\delta = 131.8$  ppm were attributed to the hydrogen and the nitrogen of the amide group, respectively. The NMR data of compounds 3–4 (Table 4) were in conformity. As demonstrated, only the <sup>1</sup>H-<sup>15</sup>N HSQC and <sup>1</sup>H-<sup>15</sup>N HMBC data lead to an unequivocal structural characterisation of compounds 2–4. Based on these observations, we can conclude that 4-hydroxy tautomer is the single species present in DMSO. Due to compounds' solubility limits, it was not possible to record the NMR spectra in other solvents, namely D<sub>2</sub>O and CDCl<sub>3</sub>.

2D NOESY experiments were also carried out for compounds 2–4. The data showed, for all compounds, an interaction between the peaks around 13 ppm (assigned by us to 4-OH) with the residual peak of water from DMSO-*d*<sub>6</sub>. This type of 2D NMR spectroscopy allowed to unequivocally assign the 3'-CH<sub>3</sub> and 4'-CH<sub>3</sub> groups of compound 2 (Table S1 and Figure S2, supporting information).

## 4. Computational studies on enzyme-ligand complexes

Taken into consideration the biological data and the previous data, molecular modelling studies were performed to investigate the binding mode of the *N*-phenyl-4-oxoquinoline-3-carboxamides (compounds 2–4) and *N*-phenyl-1-methyl-4-oxoquinoline-3-carboxamides (compounds 8–10) towards *h*MAOs. The data showed that all the compounds recognised both *h*MAOs but displayed the best values of both interaction (G-Score) and binding free energy ( $\Delta G_{\text{bind}}$ ) towards the *h*MAO-B (Table S2). In particular, the analysis of the different free energy components for each docking complex showed that VdW strongly favoured *h*MAO-B binding compared to *h*MAO-A (Table S2). The lower affinity of the compounds towards *h*MAO-A can also be explained through the formation of unfavourable steric contacts in the binding pocket,

**Table 3**  
<sup>1</sup>H and <sup>13</sup>C NMR data of compounds 2–4.


Atom number	Compound 2 (R <sub>1</sub> = R <sub>2</sub> = CH <sub>3</sub> )		Compound 3 (R <sub>1</sub> = Cl; R <sub>2</sub> = H)		Compound 4 (R <sub>1</sub> = R <sub>2</sub> = Cl)	
	Chemical shift, (ppm, DMSO- <i>d</i> <sub>6</sub> )					
	$\delta$ <sup>1</sup> H (mult, J, Hz)	$\delta$ <sup>13</sup> C	$\delta$ <sup>1</sup> H (mult, J, Hz)	$\delta$ <sup>13</sup> C	$\delta$ <sup>1</sup> H (mult, J, Hz)	$\delta$ <sup>13</sup> C
2	8.85 (s)	<u>143.9</u>	8.88 (s)	<u>144.2</u>	8.86 (s)	<u>144.5</u>
4	—	176.2	—	176.2	—	176.2
5	8.33 (dd, J = 8.4, 1.2)	<u>125.3</u>	8.33 (ddd, J = 8.1, 1.5, 0.5)	<u>125.4</u>	8.33 (dd, J = 6.9, 1.1)	<u>125.4</u>
8	7.75 (dd, J = 8.4, 1.2)	<u>119.1</u>	7.76 (ddd, J = 8.1, 1.5, 0.5)	<u>119.2</u>	7.75 (d, J = 8.2)	<u>119.7</u>
4-OH	12.90 (s)	—	12.99 (s)	—	12.99 (broad)	—
CONH	12.35 (s)	162.4	12.64 (s)	163.1	12.68 (s)	163.4

Distortionless enhancement by polarization transfer (DEPT) signals are reported as underlined values. For more information, see Table S1 (supporting information).

especially with residues Phe 208, Cys 323, Asn 181 and Ala 111, which are replaced in the isoform B with Ile199, Thr314, Cys 172 and Pro 102, respectively (Figure S3, supporting information). In the *h*MAO-A pocket, all compounds exhibited a similar binding geometry characterised by the heterocycle ring facing towards FAD (Figure S3, supporting information), except for the docking pose of compound 4.

Regarding the *h*MAO-B, two distinct binding geometries for *N*-phenyl-4-oxoquinoline-3-carboxamides (compounds 2–4) and *N*-phenyl-1-methyl-4-oxoquinoline-3-carboxamides (compounds 8–10) were observed (Fig. 6). The *N*-phenyl-4-hydroxyquinoline-3-carboxamides maintained the same binding pose, characterised by the heterocycle ring facing FAD (Fig. 6A–C). However, for compound 4, the only active compound of the series, the complex was

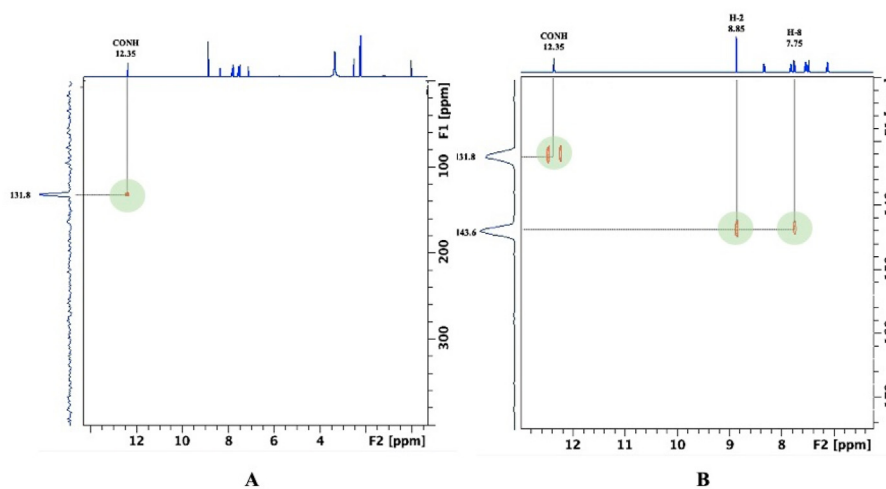
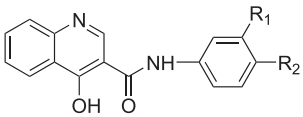
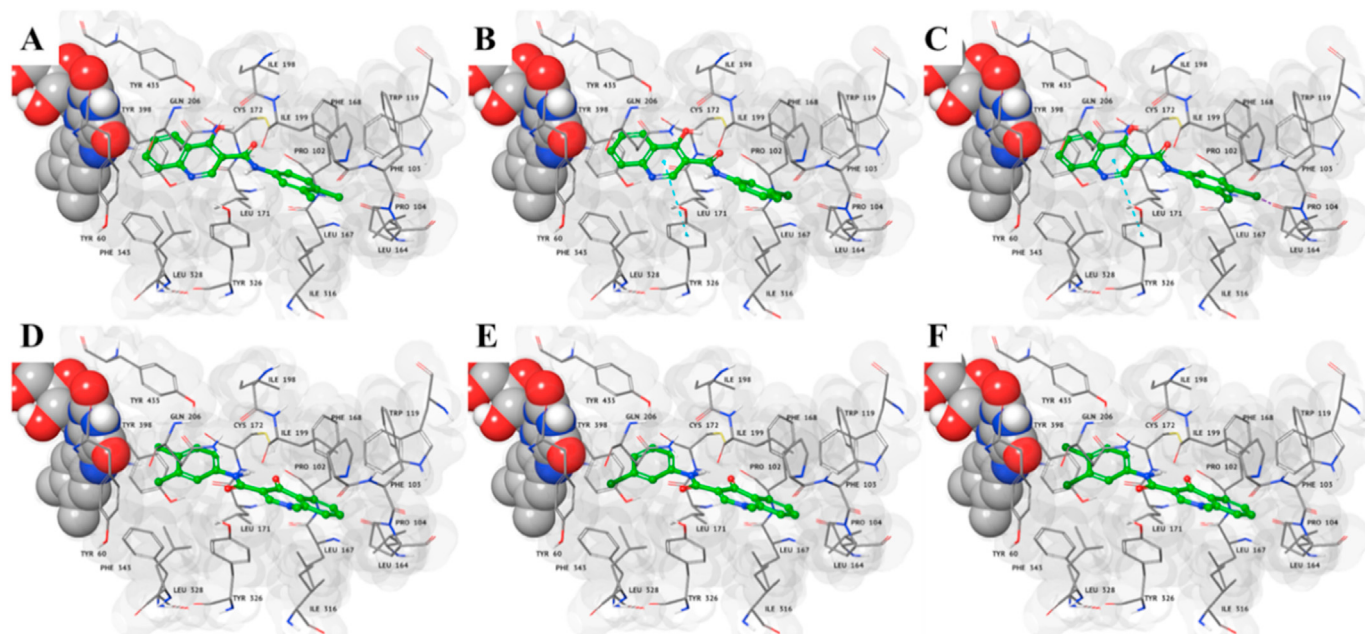


Fig. 5. (A) Expansion of <sup>1</sup>H–<sup>15</sup>N HSQC and (B) <sup>1</sup>H–<sup>15</sup>N HBMBC spectra of compound 2.

**Table 4**  
<sup>1</sup>H–<sup>15</sup>N HSQC and <sup>1</sup>H–<sup>15</sup>N HMBC data of compounds 2–4.


Compound	<sup>15</sup> N-HSQC		<sup>15</sup> N-HMBC	
	<sup>1</sup> H (ppm)	<sup>15</sup> N (ppm)	<sup>1</sup> H (ppm)	<sup>15</sup> N (ppm)
2	12.35 (CONH)	131.8	8.85 (H2) 7.74 (H8)	143.6
3	12.65 (CONH)	131.3	8.88 (H2) 7.76 (H8)	144.7
4	12.68 (CONH)	130.5	8.86 (H2) 7.75 (H8)	146.1



**Fig. 6.** 3D representation of the lowest energy complexes with *hMAO-B*, obtained after MM-GBSA calculation, for compounds: (A) 2, (B) 3, (C) 4, (D) 8, (E) 9 and (F) 10. Ligands are shown in green carbon ball-and-sticks, while the protein is represented as grey surface and FAD in CPK. Halogen and  $\pi$ - $\pi$  interaction are displayed as violet lines and dashed cyan, respectively. Amino acid residues involved in the molecular interactions are shown as grey carbon sticks.

stabilised by a  $\pi$ - $\pi$  interaction between the quinoline ring and the side chain of Tyr326, and by a halogen bond occurring between the chlorine located in a *meta*-position and the Leu164 (Fig. 6C). Moreover, for compound 4 we observed a superior number of hydrophobic interactions, when compared to compounds 2 and 3 (Fig. 6A–C), as also pointed out by the  $\Delta G_{\text{bind Lipo}}$  (Table S2).

Conversely, the *N*-phenyl-1-methyl-4-oxoquinoline-3-carboxamides (compounds 8–10) showed an opposite geometry, characterised by the heterocycle ring facing the residues Trp 119, Leu164, Leu 167, and Phe 168, which are part of the highly hydrophobic region of the entrance cavity in the enzyme (Fig. 6D–F).

Comparing the docked conformations of the ligand-enzymes complexes with the related global minimum energy, the two series of the compounds under study showed a completely different behaviour. As the global minimum energy conformers of compounds 2–4 and 8–10, are characterised by the formation of an intramolecular H-bond between the amidic NH and the oxygen at C-4 of the quinoline ring we have measured the dihedral angle ( $\chi$ ) consisting of C3', CO, NH and C1. For compounds 8–10 we observed that  $\chi$  assumed the value of  $180^\circ$  allowing a high degree of “flatness” of quinoline ring with respect to amide portion (Figure S4D–F, supporting information). Conversely, for compounds 2–4 this angle is modestly reduced ( $178.7^\circ$ ) (Figure S4D–F, supporting information).

Further docked conformer analysis demonstrated that compounds 8–10 bind to the *hMAO-B* pocket with a conformation very close to their related minimum energy (Fig. 6D–F and S4D–F, supporting information). In fact, along with their interaction with the *hMAO-B* binding pocket, they maintained the intramolecular H-bond (dihedral angle  $\chi$  values around  $175.0^\circ$ – $173.9^\circ$ ) with a high degree of planarity (Fig. 6D–F). On the other hand, docked compounds 2–4 conformations show a flip of amide portion with respect to the related minimum energy one (Fig. 6 and S4). This structural change leads to the establishment of an intramolecular H-bond between the carbonyl and the hydroxyl groups in compounds 2 and 4. For these compounds, we also observed a greater

change of dihedral angle  $\chi$  values, ranging to  $158.9^\circ$  and  $163.3^\circ$ , by resulting in a lower flatness, when compared to *N*-phenyl-1-methyl-4-oxoquinoline-3-carboxamides (compounds 8–10). Accordingly, these studies suggest that for this type of derivatives, a remarkable conformational preorganisation occurred during the *hMAO-B* recognition process.

Finally, the lowest energy complexes with *hMAO-B*, obtained after MM-GBSA calculations, were submitted to explicit water solvent molecular dynamic (MD) simulations. By analysing the RMSD plot of each ligand (Figure S5), we observed a preserved binding mode with an average RMSD value around 2 Å. Only compound 2 exhibited a different behaviour, having regard to its Root Mean Square Deviation (RMSD) values higher than 4 Å and therefore a less geometrical stability after 90 ns of MD simulation Å. Thus, the enzyme-ligand interactions occurring more than 30.0% in the 200 ns of the trajectory were monitored (Fig. 7). Interestingly, for all active compounds we observed the establishment of productive H-bonds through their amide portion. In particular, in the case of *N*-phenyl-1-methyl-4-oxoquinoline-3-carboxamides (compounds 8–10) the target-ligand complex is stabilised by the formation of an H-bond between the carbonyl group at position C-4 and the side chain of Tyr326 and/or Gln 206 (Fig. 7D–F). For the most potent IMAO-B (compound 10) the analysis also revealed an additional  $\pi$ - $\pi$  interaction between its phenyl group and the Tyr398. Remarkably, compound 4 was the unique *N*-phenyl-4-hydroxyquinoline-3-carboxamide able to establish an H-bond between its amidic nitrogen and the side chain of Ile199, two  $\pi$ - $\pi$  interactions with Tyr326 and Phe 343 and additional hydrophobic interactions (Fig. 7C).

Convincingly, during the MD simulation, we observed that the intramolecular H-bond between the amidic NH and the 4-oxoquinoline core is preserved for more than 94%. Conversely, in the hydroxyl derivatives the intramolecular H-bond occurs less than 53%, causing a loss of flatness.

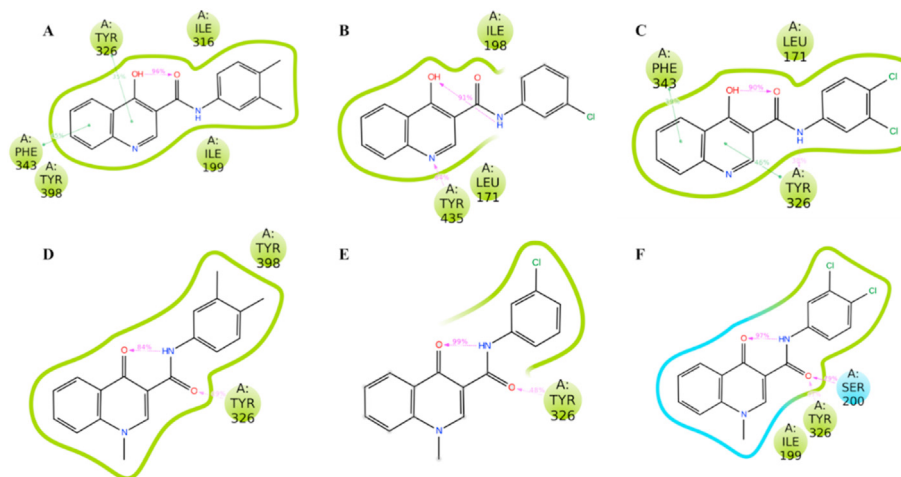


**Fig. 7.** Ligand atom interactions with the protein residues, for compounds (A) 2, (B) 3, (C) 4, (D) 8, (E) 9, and (F) 10. Only interactions that occur more than 30.0% of the simulation time in 200 ns of the trajectory are shown.

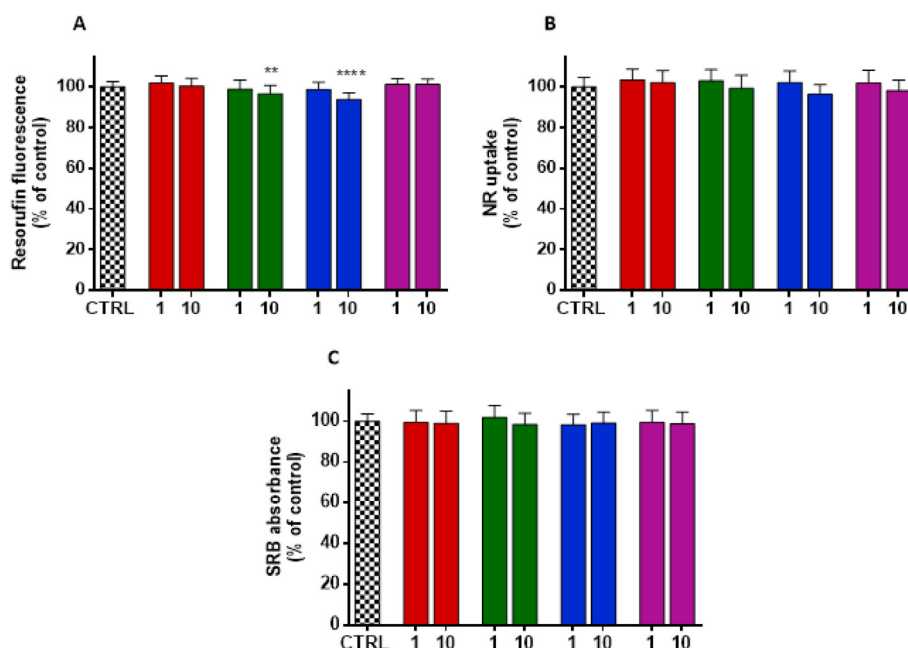


**Fig. 8.** Cellular viability of differentiated SH-SY5Y cell line after incubation for 24 h with compounds 4 (red data), 8 (green data), 9 (blue data) and 10 (purple data) at 1 and 10  $\mu\text{M}$ . Cellular viability was assessed by measuring (A) metabolic and (B) lysosomal activities and (C) cell density using resazurin reduction, neutral red (NR) uptake and sulforhodamine-B (SRB) methods, respectively. Results are represented as mean  $\pm$  SD from at least three independent experiments, performed in triplicate. Statistical comparisons were performed by using the two-way ANOVA. In all cases, p values lower than 0.05 were considered significant (\*\*p < 0.01, \*\*\*\*p < 0.001 vs control cells).

## 5. Evaluation of cytotoxic profile

The cytotoxicity of compounds 4, 9–10 was evaluated in differentiated human neuroblastoma (SH-SY5Y) cell lines, as they are often used to assess the safety potential of CNS-drug candidates [37,38]. The SH-SY5Y cells were incubated with the compounds at 1 and 10  $\mu\text{M}$  for 24 h. The cell viability was evaluated by measuring cell density, lysosomal, and mitochondrial activities using sulforhodamine-B (SRB), neutral red (NR) uptake, and resazurin reduction assays, respectively [39,40]. The results obtained (Fig. 8) are expressed as mean (% of control)  $\pm$  standard deviation (SD) of three independent experiments ( $n = 3$ ).

The data showed that all compounds at both concentrations did not alter the NR uptake or the SRB absorbance (Fig. 8B and C), when

compared to the control cells, meaning that both lysosomal activity and density of the cells were not affected. In terms of metabolic activity (Fig. 8A), despite the significant difference observed in resazurin reduction for compounds 9 ( $p < 0.001$ ) and 10 ( $p < 0.0001$ ) at the highest concentration (10  $\mu\text{M}$ ), the values obtained were higher than 90%. This slight decrease in metabolic activity can be related to an alteration of the mitochondrial activity [41].

Furthermore, the drug-like properties of the active derivatives (Compound 4, 8–10) were also calculated. Physicochemical parameters including molecular weight (MW), topological polar surface area (TPSA in  $\text{\AA}^2$ ), number of hydrogen acceptors (HBA), number of hydrogen donors (HBD), and number of rotatable bonds (RB) were estimated. Overall, the values obtained for the tested

compounds were in line with the general drug-likeness requirements of the CNS-active drugs (Table S3). In particular, the estimated LogBB value suggested the ability of the quinoline derivatives to cross the BBB and reach the CNS (Table S3).

## 6. Conclusions

The synthesis, biological evaluation, and cytotoxicity profile of a small set of *N*-phenyl-quinoline-3-carboxamides derivatives was successfully accomplished. The screening assays against MAOs isoforms showed that compounds 2 and 3 were not active at the highest concentration tested and that compound 10 was the most potent and selective IMAO-B ( $IC_{50} = 5.30 \pm 0.74$  nM and SI:  $\geq 1887$ ). No significant cytotoxic effects in differentiated SH-SY5Y cells were observed for the most active compounds in the range of concentration tested.

Moreover, we found that the prototropic tautomerism of compounds 2–4, which is blocked in compounds 8–10, markedly influenced the MAO-B inhibitory activity. The unequivocally characterisation of the type of tautomer present in solution was only possible by using 2D NMR  $^1H$ – $^{15}N$  HSQC and  $^1H$ – $^{15}N$  HMBC techniques. Computational studies and explicit water solvent MD simulations on enzyme-ligand complexes supported the experimental data. Interestingly quinolones have a dissimilar binding pose in MAO-B active site than chromones.

To our knowledge, there have been no prior reports on the characterisation of quinolone tautomers by  $^1H$ – $^{15}N$  HSQC and  $^1H$ – $^{15}N$  HMBC, which were shown to be valid and expedite tools for drug discovery programs, in which tautomerism of the chemical libraries is foreseen.

## 7. Experimental section

### 7.1. Synthesis of quinoline derivatives

#### 7.1.1. Synthesis of *N*-phenyl-4-hydroxyquinoline-3-carboxamides (2–4)

**General Procedure.** To a solution of 4-oxo-quinoline-3-carboxylic acid (1) (1.05 mmol), TBTU (1.05 mmol), DIPEA (2.1 mmol) in DMF (10 mL) the appropriate aromatic amine (1.26 mmol) was added. The reaction was stirred at room temperature overnight. Then, the mixture was diluted with DCM (50 mL), extracted with  $H_2O$  ( $3 \times 15$  mL), HCl 1 M ( $3 \times 15$  mL), and  $NaHCO_3$  saturated solution ( $3 \times 15$  mL). The combined organic phases were dried over  $Na_2SO_4$  anhydrous, filtered, and concentrated under reduced pressure. The crude product was purified by recrystallisation.

*N*-(3,4-Dimethylphenyl)-4-hydroxyquinoline-3-carboxamide (2). The compound was recrystallized from MeOH and obtained in 80% yield.  $^1H$  NMR (400 MHz,  $DMSO-d_6$ ):  $\delta$  12.90 (1H, s, OH), 12.35 (1H, s, CONH), 8.85 (1H, s, H2), 8.33 (1H, dd,  $J = 8.4, 1.2$  Hz, H5), 7.81 (1H, ddd,  $J = 8.4, 6.9, 1.2$  Hz, H6), 7.75 (1H, dd,  $J = 8.4$  Hz, 1.2 Hz, H8), 7.53 (1H, ddd,  $J = 8.4, 6.9, 1.2$  Hz, H7), 7.51 (1H, dd,  $J = 8.0, 2.1$  Hz, H6'), 7.47 (1H, d,  $J = 2.1$  Hz, H2'), 7.11 (1H, d,  $J = 8.0$  Hz, H5'), 2.23 (3H, s, 3'CH<sub>3</sub>), 2.19 (3H, s, 4'CH<sub>3</sub>).  $^{13}C$  NMR (100 MHz,  $DMSO-d_6$ )  $\delta$  176.2 (C4), 162.4 (CONH), 143.9 (C2), 139.1 (C4a), 136.6 (C1'), 136.5 (C3'), 132.8 (C6), 131.0 (C4'), 129.8 (C5'), 125.8 (C8a), 125.3 (C5), 125.1 (C7), 120.6 (C2'), 119.1 (C8), 116.8 (C6'), 110.7 (C3), 19.5 (3'CH<sub>3</sub>), 18.7 (4'CH<sub>3</sub>). MS/EI  $m/z$  (%): 89 (8), 106 (13), 116 (13), 117 (6), 119 (12), 121 (100), 122 (9), 172 (25), 292 ( $M^+$ , 6).

*N*-(3-Chlorophenyl)-4-hydroxyquinoline-3-carboxamide (3). The compound was recrystallized from MeOH and obtained in 48% yield.  $^1H$  NMR (400 MHz,  $DMSO-d_6$ ):  $\delta$  12.99 (1H, s, OH), 12.64 (1H, s, CONH), 8.88 (1H, s, H2), 8.33 (1H, ddd,  $J = 8.1, 1.5, 0.5$  Hz, H5), 8.05 (1H, dd,  $J = 2.0, 2.0$  Hz, H2'), 7.82 (1H, ddd,  $J = 8.1, 6.9, 1.5$  Hz, H6),

7.76 (1H, ddd,  $J = 8.1, 1.5, 0.5$  Hz, H8), 7.55 (1H, ddd,  $J = 8.1, 6.9, 1.5$  Hz, H7), 7.51 (1H, ddd,  $J = 8.0, 2.0, 1.0$  Hz, H6'), 7.39 (1H, dd,  $J = 8.0, 8.0$  Hz, H5'), 7.15 (1H, ddd,  $J = 8.0, 2.0, 1.0$  Hz, H4').  $^{13}C$  NMR (100 MHz,  $DMSO-d_6$ )  $\delta$  176.2 (C4), 163.1 (CONH), 144.2 (C2), 140.1 (C1'), 139.0 (C4a), 133.2 (C3'), 133.0 (C6), 130.5 (C5'), 125.8 (C8a), 125.4 (C5), 125.3 (C7), 123.0 (C4'), 119.2 (C8), 119.0 (C2'), 118.0 (C6'), 110.1 (C3). MS/EI  $m/z$  (%): 89 (16), 116 (25), 127 (77), 129 (25), 172 (100), 298 ( $M^+$ , 58), 300 ( $M+2$ , 19).

*N*-(3,4-Dichlorophenyl)-4-hydroxy-1,4-dihydroquinoline-3-carboxamide (4). The compound was recrystallized from MeOH and obtained in 35% yield.  $^1H$  NMR (400 MHz,  $DMSO-d_6$ )  $\delta$  12.68 (1H, s, CONH), 8.86 (1H, s, H2), 8.33 (1H, dd,  $J = 6.9, 1.1$  Hz, H5), 8.20 (1H, d,  $J = 1.4$  Hz, H2'), 7.82 (1H, dd,  $J = 6.9, 1.1$  Hz, H5'), 7.75 (1H, d,  $J = 8.2$  Hz, H8), 7.61–7.56 (2H, m, H6, H6'), 7.54 (1H, dd,  $J = 8.2, 6.9$  Hz, H7).  $^{13}C$  NMR ( $DMSO-d_6$ )  $\delta$  176.2 (C4), 163.4 (CONH), 144.5 (C2), 139.3 (C4a), 138.8 (C1'), 133.1 (C6), 130.8 (C5'), 125.9 (C8a), 125.4 (C5), 120.9 (C2'), 119.7 (C8), 119.4 (C6'), 110.0 (C3), C7, C3', C4' were not possible to assign. MS/EI  $m/z$  (%): 77 (26), 103 (11), 115 (36), 131 (18), 159 (100), 160 (12), 319 (12).

#### 7.1.2. Synthesis of ethyl-4-oxo-1,4-dihydroquinoline-3-carboxylate (5)

A mixture of aniline (10.73 mmol) and DEEMM (10.73 mmol) was heated at 120 °C for 1 h. After cooling the solid obtained was dissolved in diphenyl ether (32 mL). The reaction was refluxed for 2 h. After cooling, diethyl ether (25 mL) was added and the solid was filtered and recrystallized from DMF (yield 80%).  $^1H$  NMR (400 MHz,  $DMSO-d_6$ )  $\delta$ : 12.31 (1H, s, NH), 8.55 (1H, s, H2), 8.16 (1H, dd,  $J = 7.6, 1.5, 0.6$  Hz, H5), 7.71 (1H, dd,  $J = 7.6, 6.9, 1.5$  Hz, H7), 7.62 (1H, dd,  $J = 7.6, 1.5, 0.6$  Hz, H8), 7.42 (1H, dd,  $J = 7.6, 6.9$  Hz, H6), 4.22 (2H, q,  $J = 7.1$  Hz, CH<sub>2</sub>), 1.29 (3H, t,  $J = 7.1$  Hz, CH<sub>3</sub>).

#### 7.1.3. Synthesis of ethyl-1-methyl-4-oxo-1,4-dihydroquinoline-3-carboxylate (6)

Ethyl-4-oxo-1,4-dihydroquinoline-3-carboxylate (5) (1.15 mmol) and DMF (5 mL) were placed in a round bottom flask. Then,  $K_2CO_3$  (1.72 mmol) was added, and the reaction was stirred at room temperature in argon atmosphere. At that time,  $CH_3I$  (2.30 mmol) was introduced dropwise. The reaction was stirred at 60 °C for 1 h. After, the mixture was diluted with water and extracted with DCM ( $3 \times 15$  mL). The combined organic layers were dried over anhydrous  $Na_2SO_4$ , and the solvent was evaporated under reduced pressure. The crude product was crystallised from DCM (70% yield).  $^1H$  NMR (400 MHz,  $CDCl_3$ )  $\delta$ : 8.53 (1H, dd,  $J = 8.0, 1.6, 0.6$  Hz, H5), 8.46 (1H, s, H2), 7.70 (1H, dd,  $J = 8.6, 7.2, 1.6$  Hz, H7), 7.49–7.39 (2H, m, H8, H6) 4.40 (2H, q,  $J = 7.1$  Hz, CH<sub>2</sub>), 3.88 (3H, s, NCH<sub>3</sub>), 1.42 (3H, t,  $J = 7.1$  Hz, CH<sub>3</sub>).

#### 7.1.4. Synthesis of 1-methyl-4-oxo-1,4-dihydroquinoline-3-carboxylic acid (7)

A suspension of ethyl-1-methyl-4-oxo-1,4-dihydroquinoline-3-carboxylate (6) (4.41 mmol) in 10% aq. NaOH (12 mL) was refluxed for 4 h. After cooling to room temperature, the mixture was acidified with conc. HCl until pH 3. The resulting solid was filtered and washed with water (95% yield).  $^1H$  NMR (400 MHz,  $DMSO-d_6$ )  $\delta$ : 15.26 (1H, s, COOH), 9.06 (1H, s, H2), 8.39 (1H, dd,  $J = 8.1, 1.5, 0.7$  Hz, H5), 8.04–7.94 (2H, m, H7, H8), 7.70 (1H, dd,  $J = 8.1, 6.2, 1.8$  Hz, H6), 4.11 (3H, s, NCH<sub>3</sub>).

#### 7.1.5. Synthesis of *N*-phenyl-1-methyl-4-oxo-1,4-dihydroquinoline-3-carboxamides (8–10)

**General Procedure.** The *N*-phenyl-1-methyl-4-oxo-1,4-dihydroquinoline-3-carboxamides (8–10) were synthesised following the general procedure previously described for compounds 2–4, by using 1-methyl-4-oxo-1,4-dihydroquinoline-3-

carboxylic acid (7) as starting material.

*N*-(3,4-Dimethylphenyl)-1-methyl-4-oxo-1,4-dihydroquinoline-3-carboxamide (8). The compound was recrystallized from DCM and obtained in 58% yield.  $^1\text{H}$  NMR (400 MHz, DMSO- $d_6$ )  $\delta$ : 12.29 (1H, s, CONH), 8.97 (1H, s, H2), 8.41 (1H, dd,  $J = 8.1, 1.4$  Hz, H5), 7.95–7.85 (2H, m, H8, H7), 7.62 (1H, dd,  $J = 8.1, 6.4, 1.6$  Hz, H6), 7.52 (1H, dd,  $J = 8.1, 2.3$  Hz, H6'), 7.45 (1H, d,  $J = 2.3$  Hz, H2'), 7.11 (1H, d,  $J = 8.1$  Hz, H5'), 4.07 (3H, s, NCH<sub>3</sub>), 2.23 (3H, s, 3'CH<sub>3</sub>), 2.19 (3H, s, 4'CH<sub>3</sub>).  $^{13}\text{C}$  NMR (100 MHz, DMSO- $d_6$ )  $\delta$ : 176.2 (C4), 162.7 (CONH), 149.7 (C2), 140.4 (C8a), 137.2 (C3'), 137.0 (C4'), 133.7 (C7), 131.7 (C1'), 130.3 (C5'), 127.2 (C4a), 126.5 (C5), 125.9 (C6), 121.2 (C2'), 118.2 (C8), 117.5 (C6'), 111.0 (C3), 41.9 (NCH<sub>3</sub>), 20.0 (3'CH<sub>3</sub>), 19.3 (4'CH<sub>3</sub>). MS/EI  $m/z$  (%): 63 (11), 89 (22), 101 (21), 173 (100), 174 (10), 333 (12), 335 (9).

*N*-(3-Chlorophenyl)-1-methyl-4-oxo-1,4-dihydroquinoline-3-carboxamide (9). The compound was recrystallized from DCM and obtained in 80% yield.  $^1\text{H}$  NMR (400 MHz, DMSO- $d_6$ )  $\delta$ : 12.59 (1H, s, CONH), 9.00 (1H, s, H2), 8.41 (1H, dd,  $J = 8.1, 1.5, 0.6$  Hz, H5), 8.04 (1H, dd,  $J = 2.0, 2.0$  Hz, H2'), 7.96–7.87 (2H, m, H8, H7), 7.63 (1H, dd,  $J = 8.1, 6.4, 1.6$  Hz, H6), 7.52 (1H, dd,  $J = 8.1, 2.0, 1.0$  Hz, H6'), 7.39 (1H, dd,  $J = 8.1, 7.8$  Hz, H5'), 7.15 (1H, dd,  $J = 7.8, 2.0, 1.0$  Hz, H4'), 4.08 (3H, s, NCH<sub>3</sub>).  $^{13}\text{C}$  NMR (100 MHz, DMSO- $d_6$ )  $\delta$ : 175.6 (C4), 162.8 (CONH), 149.4 (C2), 140.1 (C8a), 139.8 (C1'), 133.3 (C3'), 133.2 (C7), 130.6 (C5'), 126.6 (C4a), 125.9 (C5), 125.5 (C6), 123.0 (C4'), 119.0 (C8), 118.0 (C2'), 117.7 (C6'), 109.9 (C3), 41.4 (NCH<sub>3</sub>). MS/EI  $m/z$  (%): 103 (10), 130 (18), 186 (100), 312 (M+, 28), 313 (6), 314 (M+2, 9).

*N*-(3,4-Dichlorophenyl)-1-methyl-4-oxo-1,4-dihydroquinoline-3-carboxamide (10). The compound was recrystallized from MeOH and obtained in 83% yield.  $^1\text{H}$  NMR (400 MHz, DMSO- $d_6$ )  $\delta$ : 12.66 (1H, s, CONH), 9.00 (1H, s, H2), 8.41 (1H, dd,  $J = 8.4, 1.5$  Hz, H5), 8.21–8.20 (1H, m, H2'), 7.97–7.86 (2H, m, H8, H5'), 7.63 (1H, dd,  $J = 8.2, 6.5, 1.5$  Hz, H7), 7.62–7.60 (2H, m, H6, H6'), 4.09 (3H, s, NCH<sub>3</sub>).  $^{13}\text{C}$  NMR (100 MHz, DMSO- $d_6$ )  $\delta$ : 175.6 (C4), 163.0 (CONH), 149.4 (C2), 139.9 (C8a), 138.7 (C1'), 133.3 (C7), 131.1 (C3'), 130.7 (C2'), 126.6 (C4a), 125.9 (C5), 125.6 (C6), 124.7 (C4'), 120.8 (C6'), 119.7 (C5'), 117.7 (C8), 109.7 (C3), 41.4 (NCH<sub>3</sub>). MS/EI  $m/z$  (%): 63 (4), 77 (10), 103 (14), 115 (4), 130 (25), 131 (7), 158 (8), 186 (100), 187 (12), 346 (30), 347 (M+, 6), 348 (20), 349 (M+2, 4).

## 7.2. Enzymatic assays

### 7.2.1. Evaluation of hMAOs inhibitory profile

The inhibitory activity of the selected compounds towards hMAO-A and hMAO-B was assessed using an experimental protocol previously described [21]. (See SI).

### 7.2.2. Evaluation of hMAOs oxidases kinetics

The enzymatic activity of both isoforms was studied in the presence of six different concentrations of kynuramine (10–100  $\mu\text{M}$ ) to determine the steady-state kinetic parameters ( $K_m$ , Michaelis constant, and  $V_{max}$ , maximum velocity) of hMAO-A and hMAO-B. (See SI).

## 7.3. In vitro toxicology

### 7.3.1. Cell line and culture conditions

Human neuroblastoma (SH-SY5Y) cell line was obtained from the American Type Culture Collection (ATCC, Manassas, VA, USA). SH-SY5Y cell culture and differentiation were performed as previously reported by Fernandes et al. [39] (See SI).

### 7.3.2. Evaluation of cytotoxicity profile

Stock solutions of the compounds under study (100 mM) were freshly prepared in DMSO. Final concentrations of the compounds under study were obtained by diluting into culture medium

immediately before use, giving a final maximum concentration of 0.1% DMSO. In cytotoxicity studies, the differentiated SH-SY5Y cell line was exposed to the compounds under study (1  $\mu\text{M}$  and 10  $\mu\text{M}$ ) for 24 h. Controls were treated with culture media containing 0.1% DMSO. Cell viability was estimated using three different methods: SRB, NR uptake and resazurin reduction assays. The cytotoxicity end-points were performed as described in the literature [39,40]. (See SI).

## 7.4. Modelling studies

All computer calculations were carried out by means Schrödinger Suite version 2018 [42].

### 7.4.1. Protein preparation

The crystallographic structures for both hMAO isoforms were downloaded from the Protein Data Bank (PDB) [43]. In particular, models with the PDB code 2Z5X [44] and 6FW0 [22] were selected as theoretical structures for hMAO-A and hMAO-B, respectively. For the *in silico* simulations, original PDB structures were submitted to the Protein Preparation Wizard tool [45] using OPLS2005 as force field [46]. (See SI).

### 7.4.2. Ligand preparation

The 3D structures of compounds 2–4 and 8–10 were drawn by means Maestro GUI [47]. LigPrep tools were used for modelling and calculating their protonation state at pH 7.4 [48]. (See SI).

### 7.4.3. QM-polarized ligand docking (QPLD) procedure

The co-crystallised ligands were removed in both hMAO isoforms, and a grid box of 64,000  $\text{Å}^3$  for each active target site was built by centring on the FAD N5 atom and considering a receptor van der Waals scaling of 1.0. The QM-Polarized Ligand Docking (QPLD) protocol was used for docking calculations [49–52]. (See SI) In a first step, ligands were docked into both hMAO isoforms binding site using Glide Standard Precision (SP) version 7.8 [53]; the initial charges were calculated by semi-empirical methods, and the 5 best poses for each ligand were retained. In the second step, the Quantum Mechanical (QM) treatment of charges, calculated as ESP with the semi-empirical method, allowed to take into consideration the polarization of the charges in the ligand-induced by the protein. In the final step, ligands with improved charges were redocked, retaining maximum of 10 poses per ligand. All generated complexes were submitted to Molecular Mechanics Generalized Born/Surface Area (MM-GBSA) method [54], applying molecular mechanics and continuum solvation models in order to compute their binding free energies ( $\Delta G_{\text{Bind}}$ ). Finally, for each compound, the docking pose with the best  $\Delta G_{\text{Bind}}$  was selected and analysed.

### 7.4.4. Molecular dynamics (MD)

The lowest energy complexes obtained after MM-GBSA calculation were submitted for Molecular Dynamics simulations (MDs), which were performed using Desmond software [55]. (See SI).

## Author contributions

The manuscript was written through contributions of all authors. All authors have given approval to the final version of the manuscript.

## Notes

The authors declare no competing financial interest.

## Declaration of competing interest

The authors declare that they have no known competing financial interests or personal relationships that could have appeared to influence the work reported in this paper.

## Acknowledgments

This project is supported by the Foundation for Science and Technology (FCT) and FEDER/COMPETE (Grants UID/QUI/00081/2020 and PTDC/MED-QUI/29164/2017). This article is based upon work from COST Action CA15135.

## Appendix A. Supplementary data

Supplementary data to this article can be found online at <https://doi.org/10.1016/j.ejmech.2021.113183>.

## Abbreviations

FDA Food and Drug Administration  
 MAOs Monoamine oxidases  
 CNS Central Nervous System  
 IMAO-B MAO-B inhibitors  
 PD Parkinson's disease  
 SAR Structure-Activity Relationship  
 SH-SY5Y Human neuroblastoma  
 DIPEA N,N-Diisopropylethylamine  
 TBTU 2-(1H-benzotriazole-1-yl)-1,1,3,3-tetramethylammonium tetrafluoroborate  
 DEEMM Diethyl ethoxymethylenemalonate  
 EI-MS Electronic impact mass spectrometry  
 SI Selective index  
 $\Delta G_{\text{bind}}$  Binding free energy  
 MD Molecular dynamic  
 RMSD Root Mean Square Deviation  
 SRB Sulforhodamine-B  
 NR Neutral red  
 SD Standard deviation

## References

- [1] C. Shen, A. Wang, J. Xu, Z. An, K.Y. Loh, P. Zhang, X. Liu, Recent advances in the catalytic synthesis of 4-quinolones, *Inside Chem.* 5 (2019) 1059–1107.
- [2] P. Dhiman, N. Arora, P.V. Thanikachalam, V. Monga, Recent advances in the synthetic and medicinal perspective of quinolones: a review, *Bioorg. Chem.* 92 (2019) 103291.
- [3] S. Hadida, F. Van Goor, J. Zhou, V. Arumugam, J. McCartney, A. Hazlewood, C. Decker, P. Negulescu, P.D. Grootenhuys, Discovery of N-(2,4-di-tert-butyl-5-hydroxyphenyl)-4-oxo-1,4-dihydroquinoline-3-carboxamide (VX-770, ivacafator), a potent and orally bioavailable CFTR potentiator, *J. Med. Chem.* 57 (2014) 9776–9795.
- [4] A. Mermer, N. Demirbas, Y. Sirin, H. Uslu, Z. Ozdemir, A. Demirbas, Conventional and microwave prompted synthesis, antioxidant, anticholinesterase activity screening and molecular docking studies of new quinolone-triazole hybrids, *Bioorg. Chem.* 78 (2018) 236–248.
- [5] V. Hepnarova, J. Korabecny, L. Matouskova, P. Jost, L. Muckova, M. Hrabanova, N. Vykoukalova, M. Kerhartova, T. Kucera, R. Dolezal, E. Nepovimova, K. Spilovska, E. Mezeiova, N.L. Pham, D. Jun, F. Staud, D. Kaping, K. Kuca, O. Soukup, The concept of hybrid molecules of tacrine and benzyl quinolone carboxylic acid (BQCA) as multifunctional agents for Alzheimer's disease, *Eur. J. Med. Chem.* 150 (2018) 292–306.
- [6] Z. Wang, M. Cao, H. Xiang, W. Wang, X. Feng, X. Yang, WBQ5187, a multitarget directed agent, ameliorates cognitive impairment in a transgenic mouse model of Alzheimer's disease and modulates cerebral beta-amyloid, gliosis, cAMP levels, and neurodegeneration, *ACS Chem. Neurosci.* 10 (2019) 4787–4799.
- [7] P. Ghosh, S. Das, Synthesis and functionalization of 4-quinolones – a progressing story, *Eur. J. Org. Chem.* 2019 (2019) 4466–4516.
- [8] D.E. Edmondson, C. Binda, Monoamine Oxidases, *Subcell. Biochem.* 87 (2018) 117–139.
- [9] D. Knez, M. Sova, U. Kosak, S. Gobec, Dual inhibitors of cholinesterases and monoamine oxidases for Alzheimer's disease, *Future Med. Chem.* 9 (2017) 811–832.
- [10] M.B. Youdim, D. Edmondson, K.F. Tipton, The therapeutic potential of monoamine oxidase inhibitors, *Nat. Rev. Neurosci.* 7 (2006) 295–309.
- [11] A. Gaspar, T. Silva, M. Yanez, D. Vina, F. Orallo, F. Ortuso, E. Uriarte, S. Alcaro, F. Borges, Chromone, a privileged scaffold for the development of monoamine oxidase inhibitors, *J. Med. Chem.* 54 (2011) 5165–5173.
- [12] J. Reis, F. Cagide, D. Chavarria, T. Silva, C. Fernandes, A. Gaspar, E. Uriarte, F. Remiao, S. Alcaro, F. Ortuso, F. Borges, Discovery of new chemical entities for old targets: insights on the lead optimization of chromone-based monoamine oxidase B (MAO-B) inhibitors, *J. Med. Chem.* 59 (2016) 5879–5893.
- [13] A. Fonseca, J. Reis, T. Silva, M.J. Matos, D. Bagetta, F. Ortuso, S. Alcaro, E. Uriarte, F. Borges, Coumarin versus chromone monoamine oxidase B inhibitors: quo vadis? *J. Med. Chem.* 60 (2017) 7206–7212.
- [14] R. Dhiman, S. Sharma, G. Singh, K. Nepali, P.M. Singh Bedi, Design and synthesis of aza-flavones as a new class of xanthine oxidase inhibitors, *Arch. Pharm. (Weinheim)* 346 (2013) 7–16.
- [15] X.H. Han, S.S. Hong, D. Lee, J.J. Lee, M.S. Lee, D.C. Moon, K. Han, K.W. Oh, M.K. Lee, J.S. Ro, B.Y. Hwang, Quinolone alkaloids from *evodia fructus* and their inhibitory effects on monoamine oxidase, *Arch. Pharm. Res. (Seoul)* 30 (2007) 397–401.
- [16] M.K. Lee, B.Y. Hwang, S.A. Lee, G.J. Oh, W.H. Choi, S.S. Hong, K.S. Lee, J.S. Ro, 1-Methyl-2-undecyl-4(1H)-quinolone as an irreversible and selective inhibitor of type B monoamine oxidase, *Chem. Pharm. Bull.* 51 (2003) 409–411.
- [17] S. Pasquini, L. Botta, T. Semeraro, C. Mugnaini, A. Ligresti, E. Palazzo, S. Maione, V. Di Marzo, F. Corelli, Investigations on the 4-quinolone-3-carboxylic acid motif. 2. Synthesis and structure-activity relationship of potent and selective cannabinoid-2 receptor agonists endowed with analgesic activity in vivo, *J. Med. Chem.* 51 (2008) 5075–5084.
- [18] L.R. Gomes, J.N. Low, F. Borges, A. Gaspar, F. Mesiti, The synthesis, crystal structure and Hirshfeld analysis of 4-(3,4-di-methyl-anilino)-N-(3,4-dimethyl-phen-yl)quinoline-3-carboxamide, *Acta Crystallogr E Crystallogr Commun* 76 (2020) 201–207.
- [19] S. Pasquini, C. Mugnaini, C. Tintori, M. Botta, A. Trejos, R.K. Arvela, M. Larhed, M. Witvrouw, M. Michiels, F. Christ, Z. Debyser, F. Corelli, Investigations on the 4-quinolone-3-carboxylic acid motif. 1. Synthesis and structure-activity relationship of a class of human immunodeficiency virus type 1 integrase inhibitors, *J. Med. Chem.* 51 (2008) 5125–5129.
- [20] S. Gupta, P. Ghosh, S. Dwivedi, S. Das, Synthesis of 6-aryl substituted 4-quinolones via Suzuki cross coupling, *RSC Adv.* 4 (2014) 6254–6260.
- [21] D. Chavarria, C. Fernandes, V. Silva, C. Silva, E. Gil-Martins, P. Soares, T. Silva, R. Silva, F. Remiao, P.J. Oliveira, F. Borges, Design of novel monoamine oxidase-B inhibitors based on piperine scaffold: structure-activity-toxicity, drug-likeness and efflux transport studies, *Eur. J. Med. Chem.* 185 (2020) 111770.
- [22] J. Reis, N. Manzella, F. Cagide, J. Miale-Perez, E. Uriarte, A. Parini, F. Borges, C. Binda, Tight-binding inhibition of human monoamine oxidase B by chromone analogs: a kinetic, crystallographic, and biological analysis, *J. Med. Chem.* 61 (2018) 4203–4212.
- [23] M.J. Mphahlele, F.K. Mogamisi, M. Tsanwani, S.M. Hlatshwayo, R.M. Mampa, Iodine-Methanol-promoted oxidation of 2-Aryl-1,2,3,4-tetrahydro-4-quinolones to 2-Aryl-4-methoxyquinolones, *J. Chem. Res.* (1999) 706–707.
- [24] A.R. Katritzky, J. Ellison, J. Frank, P. Rákóczy, L. Radics, E. Gács-Baitz, 13C NMR spectra of 4-quinolones and related compounds, *Org. Magn. Reson.* 16 (1981) 280–284.
- [25] P.C. Horta, M.S.C. Henriques, N. Kuş, J.A. Paixão, P.M. O'Neill, M.L.S. Cristiano, R. Fausto, Synthesis, structural and conformational analysis, and IR spectra of ethyl 4-chloro-7-iodoquinoline-3-carboxylate, *Tetrahedron* 71 (2015) 7583–7592.
- [26] O.-Y. Kang, S.J. Park, H. Ahn, K.C. Jeong, H.J. Lim, Structural assignment of the enol-keto tautomers of one-pot synthesized 4-hydroxyquinolines/4-quinolones, *Org. Chem. Front.* 6 (2019) 183–189.
- [27] M.J. Mphahlele, M.A. Fernandes, A.M. El-Nahas, H. Ottosson, S.M. Ndlovu, H.M. Sithole, B.S. Dladla, D. De Waal, Solution phase, solid state and computational structural studies of the 2-aryl-3-bromoquinolin-4(1H)-one derivatives 1, *J. Chem. Soc. Perkin. Trans. 2* (2002) 2159–2164.
- [28] C. Wentrup, V.V. Rao, W. Frank, B.E. Fulloon, D.W. Moloney, T. Mosandl, Aryliminopropadienone-C-Amidoketenimine-amidinoketene-2-aminoquinolone cascades and the ynamine-isocyanate reaction, *J. Org. Chem.* 64 (1999) 3608–3619.
- [29] A.R. Todorov, M. Nieger, J. Helaja, Tautomeric switching and metal-cation sensing of ligand-equipped 4-hydroxy-/4-oxo-1,4-dihydroquinolines, *Chemistry* 18 (2012) 7269–7277.
- [30] E. Murguly, T.B. Norsten, N. Branda, Tautomerism of 4-hydroxyterpyridine in the solid, solution and gas phases: an X-ray, FT-IR and NMR study, *J. Chem. Soc. Perkin. Trans. 2* (1999) 2789–2794.
- [31] A. De la Cruz, J. Elguero, P. Goya, A. Martínez, W. Pfeleiderer, Tautomerism and acidity in 4-quinolone-3-carboxylic acid derivatives, *Tetrahedron* 48 (1992) 6135–6150.
- [32] M. Petrova, R. Muhamedjević, B. Vígante, G. Duburs, E. Liepinsh, Intramolecular hydrogen bonds in 1,4-dihydropyridine derivatives, *R. Soc. Open. Sci.* 5 (2018) 180088.
- [33] E. Stern, G.G. Muccioli, B. Bosier, L. Hamtiaux, R. Millet, J.H. Poupaert, J.P. Henichart, P. Depreux, J.F. Goossens, D.M. Lambert, Pharmacomodulations around the 4-oxo-1,4-dihydroquinoline-3-carboxamides, a class of potent CB2-selective cannabinoid receptor ligands: consequences in receptor affinity

- and functionality, *J. Med. Chem.* 50 (2007) 5471–5484.
- [34] N. Vasudevan, G.R. Jachak, D.S. Reddy, Breaking and making of rings: a method for the preparation of 4-Quinolone-3-carb-oxylic acid amides and the expensive drug ivacaftor, *Eur. J. Org. Chem.* (2015) 7433–7437, 2015.
- [35] M.J. Mphahlele, A.M. El-Nahas, Tautomeric 2-arylquinolin-4(1H)-one derivatives- spectroscopic, X-ray and quantum chemical structural studies, *J. Mol. Struct.* 688 (2004) 129–136.
- [36] S.C. Kuo, H.Z. Lee, J.P. Juang, Y.T. Lin, T.S. Wu, J.J. Chang, D. Lednicer, K.D. Paull, C.M. Lin, Synthesis and cytotoxicity of 1,6,7,8-substituted 2-(4'-substituted phenyl)-4-quinolones and related compounds: identification as antimetabolic agents interacting with tubulin, *J. Med. Chem.* 36 (1993) 1146–1156.
- [37] Ö.N. Kanat, G. Selmanoğlu, Neurotoxic effect of fipronil in neuroblastoma SH-SY5Y cell line, *Neurotox. Res.* 37 (2020) 30–40.
- [38] M.M. Shipley, C.A. Mangold, M.L. Szpara, Differentiation of the SH-SY5Y human neuroblastoma cell line, *JoVE* (2016) 53193.
- [39] C. Fernandes, M. Pinto, C. Martins, M.J. Gomes, B. Sarmiento, P.J. Oliveira, F. Remião, F. Borges, Development of a PEGylated-based platform for efficient delivery of dietary antioxidants across the blood–brain barrier, *Bioconjugate Chem.* 29 (2018) 1677–1689.
- [40] C. Fernandes, C. Martins, A. Fonseca, R. Nunes, M.J. Matos, R. Silva, J. Garrido, B. Sarmiento, F. Remião, F.J. Otero-Espinar, E. Uriarte, F. Borges, PEGylated PLGA nanoparticles as a smart carrier to increase the cellular uptake of a coumarin-based monoamine oxidase B inhibitor, *ACS Appl. Mater. Interfaces* 10 (2018) 39557–39569.
- [41] G. Cohen, N. Kesler, Monoamine oxidase and mitochondrial respiration, *J. Neurochem.* 73 (1999) 2310–2315.
- [42] Schrödinger, LLC, NY, USA, (2018).
- [43] [www.rcsb.org](http://www.rcsb.org).
- [44] S.Y. Son, J. Ma, Y. Kondou, M. Yoshimura, E. Yamashita, T. Tsukihara, Structure of human monoamine oxidase A at 2.2-Å resolution: the control of opening the entry for substrates/inhibitors, *Proc. Natl. Acad. Sci. U. S. A.* 105 (2008) 5739–5744.
- [45] G.M. Sastry, M. Adzhigirey, T. Day, R. Annabhimoju, W. Sherman, Protein and ligand preparation: parameters, protocols, and influence on virtual screening enrichments, *J. Comput. Aided Mol. Des.* 27 (2013) 221–234.
- [46] D. Shivakumar, E. Harder, W. Damm, R.A. Friesner, W. Sherman, Improving the prediction of absolute solvation free energies using the next generation OPLS force field, *J. Chem. Theor. Comput.* 8 (2012) 2553–2558.
- [47] Maestro, Schrödinger, LLC, NY, USA, (2018).
- [48] LigPrep, Maestro, Schrödinger-Suites, LLC, NY, USA, (2018).
- [49] A.E. Cho, V. Guallar, B.J. Berne, R. Friesner, Importance of accurate charges in molecular docking: quantum mechanical/molecular mechanical (QM/MM) approach, *J. Comput. Chem.* 26 (2005) 915–931.
- [50] Schrödinger, Jaguar, LLC, NY, USA, (2016).
- [51] QSite, Schrödinger, LLC, NY, USA, (2018).
- [52] QM-Polarized, Ligand Docking Protocol, Glide, Schrödinger, LLC, NY, USA, 2016.
- [53] Glide, Schrödinger, LLC, NY, USA, (2018).
- [54] P.A. Kollman, I. Massova, C. Reyes, B. Kuhn, S. Huo, L. Chong, M. Lee, T. Lee, Y. Duan, W. Wang, O. Donini, P. Cieplak, J. Srinivasan, D.A. Case, T.E. Cheatham, Calculating structures and free energies of complex Molecules: combining molecular mechanics and continuum models, *Acc. Chem. Res.* 33 (2000) 889–897.
- [55] Desmond Molecular Dynamics System, D. E. Shaw Research, NY, USA, 2018, version 5.3.